Materials Science and Engineering A 547 (2012) 55–63

Contents lists available at SciVerse ScienceDirect

Materials Science and Engineering A

journal homepage: www.elsevier.com/locate/msea

Microstructural evolution in recrystallized and unrecrystallized Al–Mg–Sc alloys during superplastic deformation

F.C. Liu, P. Xue, Z.Y. Ma*

Shenyang National Laboratory of Materials Science, Institute of Metal Research, Chinese Academy of Sciences, 72 Wenhua Road, Shenyang 110016, China

ARTICLE INFO

Article history:
Received 1 November 2011
Received in revised form 11 January 2012
Accepted 7 March 2012
Available online 29 March 2012

Keywords:
Aluminum alloys
Superplasticity
Friction sir processing
Grain boundaries
Texture

ABSTRACT

The microstructural evolution of unrecrystallized (extruded) and recrystallized (friction stir processed, FSP) Al–Mg–Sc alloys during superplastic straining was investigated using electron backscatter diffraction (EBSD). The unrecrystallized structure gradually transformed into a recrystallized structure, characterized by equiaxed grains, random boundary misorientation distribution and a weak texture at high strains. This evolution was divided into three stages based on true stress–strain curves and EBSD maps, i.e. subgrain rotation and coalescence in the early stage, dynamic recrystallization in the middle stage, and grain boundary sliding (GBS) and dynamic grain growth in the final stage. By comparison, the recrystallized grains in the FSP Al–Mg–Sc maintained a random distribution during the whole deformation process, however the grain size increased significantly with increasing strain, indicating that the main deformation mechanism was always GBS and dynamic grain growth. A deformation model was proposed to explain the microstructural evolution during superplastic deformation. The microstructure with the random boundary misorientations reaches a dynamic balance because the transformation between high-angle grain boundaries and low-angle grain boundaries is equivalent.

1. Introduction

It is generally accepted that grain boundary sliding (GBS) is the dominant deformation mechanism during superplastic flow for most fine-grained materials when the strain rate sensitivity of flow stress is approximately 0.5 [1]. The microstructural prerequisites for GBS are an excellent combination of equiaxed, stable, fine-grained structure and, primarily, high-angle grain boundaries (HAGBs) capable of sliding during elevated temperature deformation. Furthermore, the grain boundaries should have the capability of emission and absorption of vacancies, so that the GBS can be accommodated by diffusion or diffusion-controlled processes [2].

However, rolled or extruded aluminum alloys, particularly those containing a high number density of fine particles which give rise to significant Zener pinning during processing, are generally in an unrecrystallized condition prior to superplastic deformation [3]. A fine-grained structure which confers superplastic characteristics develops from the rolled or extruded structure during the early stages of superplastic deformation [4,5]. The mechanism by which the fine-grained recrystallized structure can evolve dynamically is, however, not completely understood.

One hypothesis [6,7] proposed that fine grains appeared as a consequence of rapid subgrain growth during deformation at high temperatures. The misorientation of a grain boundary was considered to accumulate linearly with the boundary migration distance. Therefore, a HAGB could evolve from a subgrain boundary, providing that the subgrain boundary migrated a sufficient distance. This hypothesis predicts that a deformation texture is maintained, although it is somewhat weakened, after superplastic deformation. However, other studies [5,8] showed that the deformation texture became progressively more diffused with increasing strain, and finally approached a random distribution. A hypothesis for this change is that the subgrain rotation was assisted by sliding deformation, even though a study concerning bicrystals suggested that GBS is unlikely to occur between subgrains, owing to their minor differences in orientation [9].

Hales and McNelley [2] suggested that subgrain-boundary sliding would occur when the boundary misorientation reached about 5–7°. Moreover, Gudmundsson et al. [10] proposed that only HAGBs were capable of sliding at the start of the straining of polycrystalline alloys. Sliding along the preexisting HAGBs caused the rotation of the adjoining subgrains, thereby introducing additional HAGBs which are also able to slide. Repetition of this process transforms LAGBs to HAGBs throughout the microstructure.

During superplastic deformation, the unrecrystallized microstructure in the rolled or extruded aluminum alloys gradually evolved into a structure consisting of new recrystallized grains by increasing the strain. Approximately equiaxed grain structure with

* Corresponding author. Tel.: +86 24 83978908; fax: +86 24 83978908.
E-mail address: zyma@imr.ac.cn (Z.Y. Ma).

0921-5093/$ – see front matter © 2012 Elsevier B.V. All rights reserved.
http://dx.doi.org/10.1016/j.msea.2012.03.076

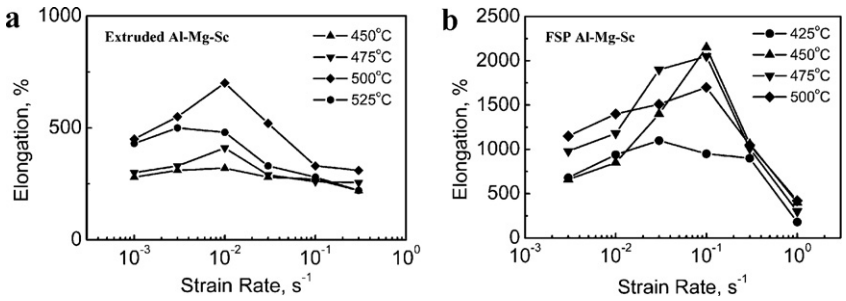

Fig. 1. Variation of elongation with initial strain rate at various temperatures for (a) extruded and (b) FSP Al–Mg–Sc.

nearly random texture and misorientation distribution appeared at the final stage of the superplastic deformation [4–6,11,12]. Liu and Chakrabarti [11] systematically studied the grain structure evolution of an unrecrystallized sheet of Sc-modified 7050Al during superplastic deformation. They asserted that a continuous evolution process occurred based on gradual boundary misorientation and microtexture evolution. The mean misorientation and the fraction of HAGBs increased rapidly beyond the stress maximum at a strain of 0.4 due to the GBS and grain rotation. However, the evolution of the grain/subgrain structure was studied by polarized light metallography, which resulted in some microstructural details being omitted.

Friction stir processing (FSP), which was developed from friction stir welding [13,14], has been demonstrated to be an effective processing technique for producing fine-grained aluminum alloys exhibiting excellent low-temperature and/or high strain rate superplasticity [15–20]. It is interesting that FSP aluminum alloys were characterized by fine recrystallized grains with a nearly random texture and misorientation distribution [17–20]. However, a systematical study of the microstructural evolution, especially on the change in the grain structure and local texture, of the FSP aluminum alloys during superplastic deformation is still lacking.

In this study, the hot extruded and FSP Al–Mg–Sc samples consisting of unrecrystallized and recrystallized grain structures, were subjected to superplastic investigation. The microstructures of the two samples at various deformation stages were characterized by the electron backscatter diffraction (EBSD) technique, which provided more detailed microstructural information than optical microscopy, and were related to the operative deformation mechanism. The objective of this study is (a) to provide a further insight into how a microstructure consisting mainly of subgrains evolves into an equiaxed grain structure, (b) to elucidate the evolution of the grain structure, misorientation distribution and local texture in the FSP aluminum alloy with nearly random texture and boundary misorientation distribution, and (c) to further understand the influence of microstructural characteristics on superplastic behavior.

2. Experimental

Al–5.33Mg–0.23Sc–0.49Mn–0.14Fe–0.06Zr (in wt%) alloy was used in this study. The alloy was initially produced by ingot casting. After a homogenization treatment at 430 °C for 24 h, the ingot was extruded into a flat plate of 8 mm × 70 mm at an extrusion ratio of 15.5:1 with a ram speed of 0.5 mm/s. A single pass FSP was carried out on the extruded plate along the extrusion direction at a tool rotation rate of 600 rpm and a traverse speed of 25 mm/min. A steel tool with a concave shoulder 14 mm in diameter, a threaded conical pin 5 mm in root diameter and 3.5 mm in tip diameter, and 4.5 mm in length was used.

Dog-bone shaped tensile specimens (2.5 mm gage length, 1.4 mm gage width and 1.0 mm gage thickness) were electro-discharge machined from the middle of the extruded sample, parallel to the extruding direction, and the SZ of the FSP sample, transverse to the FSP direction, respectively. These specimens were subsequently ground and polished to a final thickness of ~0.8 mm. Constant crosshead speed tensile tests were conducted using an INSTRON 5848 micro-tester. Each specimen was held at the testing temperature for about 15 min in order to reach thermal equilibrium. The undeformed specimens and the specimens that were pulled to different strains were examined using a ZEISS SUPRA 35 scanning electron microscope (SEM) equipped with an HKL Channel EBSD system. The EBSD examination was performed on the plane parallel to the extrusion direction for the extruded samples and on the plane perpendicular to the FSP direction for the FSP samples, respectively. Kikuchi patterns were obtained automatically at steps of 0.2–0.5 μm based on the grain sizes of the specimens. Owing to the limited angular resolution, misorientations less than 2° were not considered. The RD and the ND in the inverse pole figures represent the extrusion direction for the extruded samples and the FSP direction for the FSP samples, respectively.

3. Results

3.1. Tensile deformation

Fig. 1a shows the variation of elongation with the strain rate at different temperatures for the extruded Al–Mg–Sc. Elongation increased with an increase in the testing temperature until it reached the maximum value at 500 °C, and then decreased as the temperature increased. A maximum elongation of 700% was achieved at 500 °C and $1 \times 10^{-2}\,s^{-1}$. Fig. 1b shows the variation of elongation with the strain rate at different temperatures for the FSP Al–Mg–Sc. A temperature increase from 425 to 450 °C resulted in an increase in the optimum strain rate for superplasticity, as well as the maximum elongation. The largest elongation of 2150% was achieved at 450 °C and $1 \times 10^{-1}\,s^{-1}$. However, with an increase in temperature from 450 to 500 °C, the maximum elongation decreased from 2150% to 1700%.

Fig. 2 shows the true stress–strain (σ–ε) curves of the FSP Al–Mg–Sc sample at 450 °C and $1 \times 10^{-1}\,s^{-1}$ and the extruded Al–Mg–Sc sample at 500 °C and $1 \times 10^{-2}\,s^{-1}$, where the largest superplastic elongations were observed. The flow stress for the FSP Al–Mg–Sc showed extensive strain hardening up to a large strain. After reaching a maximum, the flow stress continuously decreased until failure. For the extruded Al–Mg–Sc, the strain hardening was only observed within the initial strain range. Then, the flow stress decreased continuously with increasing strain.

3.2. Microstructural characteristics of extruded sample at different strains

The EBSD map shows that the extruded sample contained a heavily deformed microstructure composed of banded unrecrystallized grains and fine recrystallized grains along the extruding

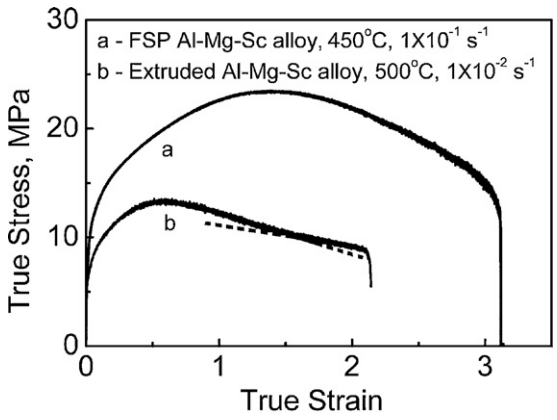

Fig. 2. True stress–strain curves for extruded and FSP Al–Mg–Sc.

direction. After static annealing at the test temperature (500 °C) for 20 min, only recovery, but no significant subgrain growth or recrystallization, occurred, as evidenced in Fig. 3a. The black and white lines represent the HAGBs (grain boundary orientation angle ≥ 15°) and low angle grain boundaries (LAGBs, grain boundary orientation angle < 15°), respectively. The HAGBs were mainly distributed on the banded boundaries, which were parallel to the extruding direction, and around the recrystallized grains. The ⟨1 1 1⟩ and ⟨1 0 0⟩ grains that dominated the microstructure are shown in blue and red, respectively.

Fig. 3b shows the frequency distribution of boundary misorientation angles for the statically annealed sample. The theoretical distribution of grain boundary misorientation angles for a random grain assembly of a cubic structure [21] is also shown by a black solid line. It is noted that the number fraction of the boundaries decreased by increasing the misorientation angle in the range of 3–15°. When the misorientation angle is greater than 15°, the grain boundary misorientation histogram is almost flat. The average misorientation angle was determined to be 21.5°. The fraction of the HAGBs was only 48%. The local texture data are shown in the form of inverse pole figures (Fig. 3c). Distinct ⟨1 1 1⟩ fiber texture aligned parallel to the extruding direction was observed. The maximum intensity is 5.05. The grain structure, misorientation distribution and texture for the as-extruded sample were similar to those for the statically annealed sample. Therefore, the microstructural data of the as-extruded sample are not shown in this study.

At a strain of 0.6, the subgrains were rearranged and the size of the subgrains increased significantly (Fig. 4a). Some large subgrains increased to nearly one hundred micrometers in length and over ten micrometers in width. Most of the HAGBs were still distributed on the banded boundaries and the boundaries of the fine equiaxed grains. Compared with the statically annealed sample, a decrease in the proportion of the LAGBs with misorientation angles of <5° occurred with a concurrent increase in the HAGBs with misorientation angles of >50°, and the corresponding misorientation histogram exhibited two peaks (Fig. 4b). There is no noticeable change in the proportion of the grain boundaries with misorientation angles of 15–50°. The average misorientation angle and the fraction of HAGBs increased to 27.3° and 58%, respectively. The inverse pole figures showed that the ⟨1 1 1⟩ fiber texture still aligned along the extruding direction but the maximum intensity was reduced to 4.70 (Fig. 4c).

At a strain of 1.6, the initial banded microstructure becomes less well defined and was replaced by a nearly equiaxed grain structure (Fig. 5a). The mean grain size of the sample was determined to be ~11.2 μm. Further observation revealed that region I was occupied by a high density of ⟨1 1 1⟩ grains, which is a character of the remaining banded structure. No noticeable misorientation concentration was observed in region II. The average misorientation angle and the fraction of HAGBs increased to 37.1° and 89%, respectively, which are close to the theoretical distribution (Fig. 5b). The inverse pole figures revealed a weak ⟨1 1 1⟩ fiber texture with a maximum density of 3.17 (Fig. 5c).

At a strain of 2.1, the microstructure was characterized by randomly distributed equiaxed grains with an average grain size of

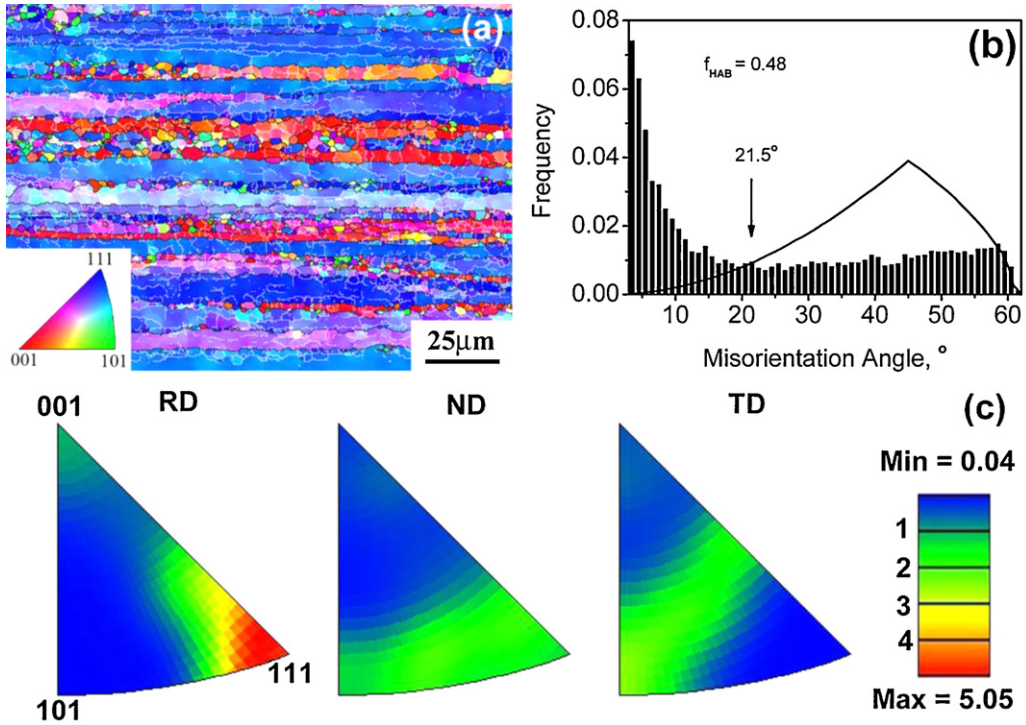

Fig. 3. Microstructure of extruded Al–Mg–Sc: (a) EBSD map, (b) boundary misorientation angle distribution, and (c) inverse pole figures.

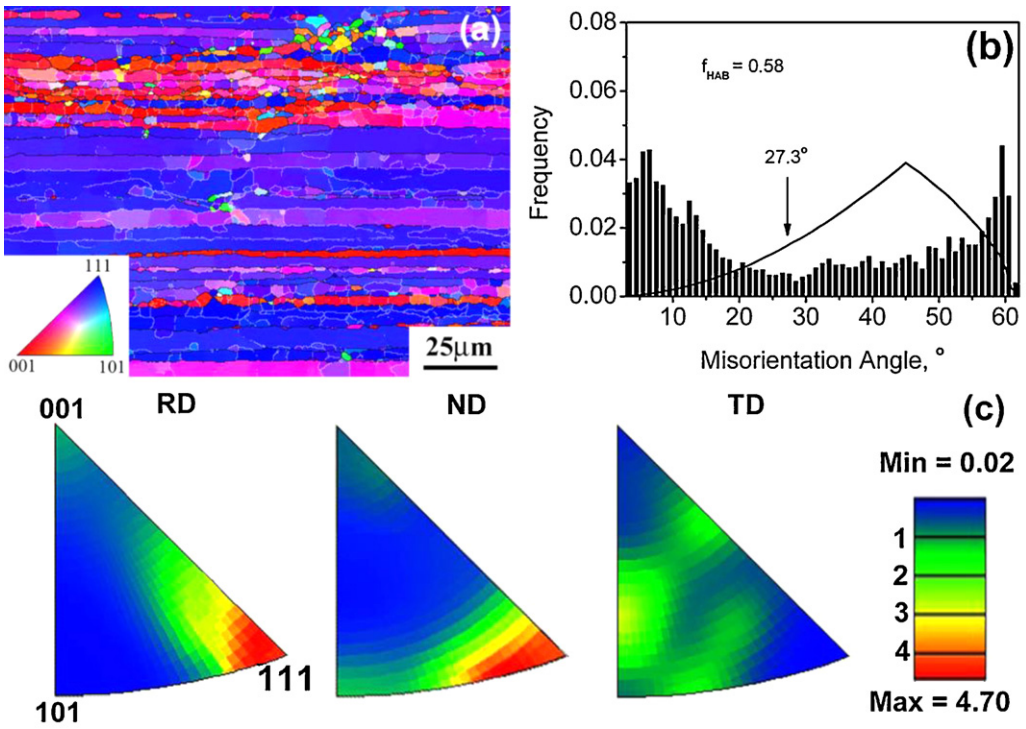

Fig. 4. Microstructure of extruded Al–Mg–Sc deformed to a strain of 0.6: (a) EBSD map, (b) boundary misorientation angle distribution, and (c) inverse pole figures.

25.5 μm (Fig. 6a). The misorientation distribution shows a close match with the theoretical distribution (Fig. 6b). The average misorientation angle and the fraction of HAGBs were 37.1° and 94%, respectively, and very close to 40.7° and 97% for the random misorientation distribution predicted by Mackenzie [21]. The maximum orientation density of the ⟨1 1 1⟩ fiber texture was only 1.81 (Fig. 6c).

3.3. Microstructural characteristics of FSP sample at different strains

Fig. 7 shows the microstructure of the FSP Al–Mg–Sc obtained by EBSD mapping. FSP produced a fully recrystallized microstructure with uniform and equiaxed grains and the average grain size was

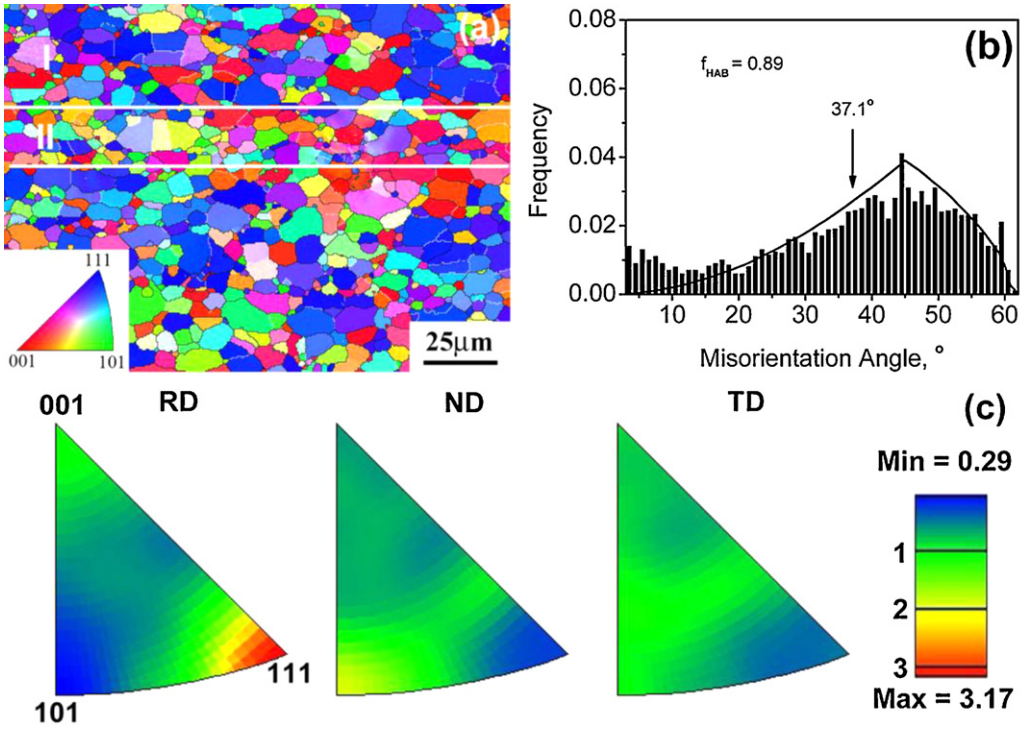

Fig. 5. Microstructure of extruded Al–Mg–Sc deformed to a strain of 1.6: (a) EBSD map, (b) boundary misorientation angle distribution, and (c) inverse pole figures.

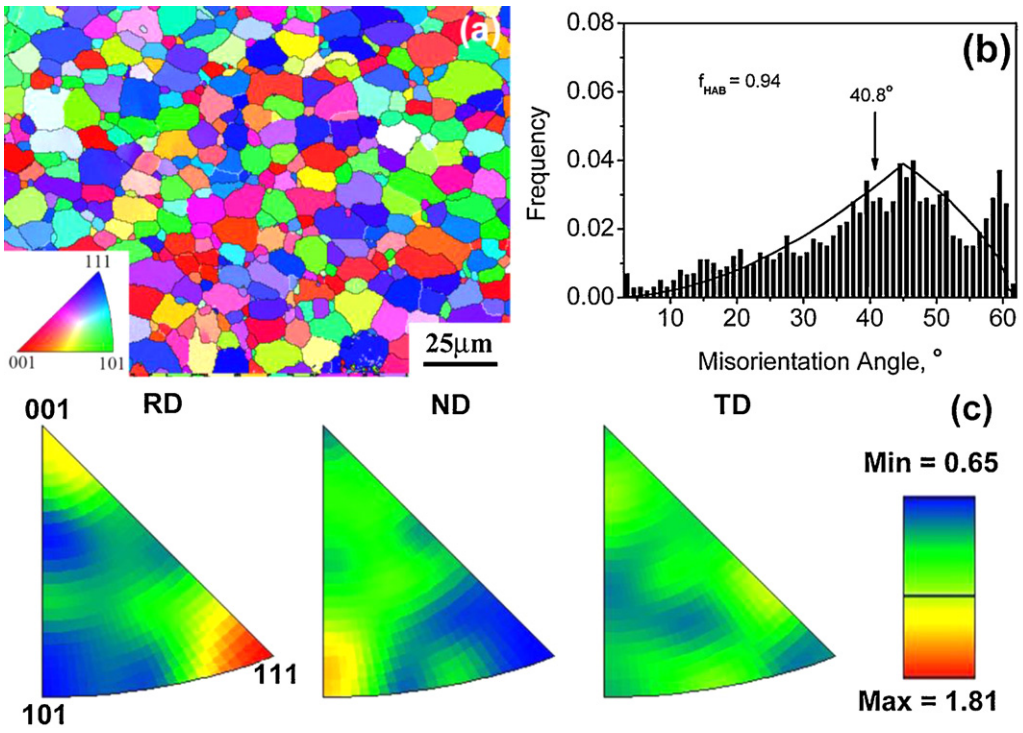

Fig. 6. Microstructure of extruded Al–Mg–Sc deformed to a strain of 2.1: (a) EBSD map, (b) boundary misorientation angle distribution, and (c) inverse pole figures.

determined to be ~2.6 μm (Fig. 7a). The misorientation distribution of the FSP sample, with an average misorientation angle of 40.3° and a HAGB fraction of 97% (Fig. 7b), is very close to the grain assembly for randomly oriented cubes [21]. Furthermore, it was discovered that the FSP Al–Mg–Sc exhibited a very weak texture component as indicated by the inverse pole figures in Fig. 7c.

Figs. 8 and 9 show the microstructure evolution of the FSP Al–Mg–Sc during superplastic deformation. By increasing the strains to 1.4 and 3.1, the grains remained equiaxed and randomly distributed, but the sizes of grains increased to 4.8 and 7.6 μm, respectively. At strains of 1.4 and 3.1, the FSP Al–Mg–Sc showed a very weak, almost random, texture while the misorientation

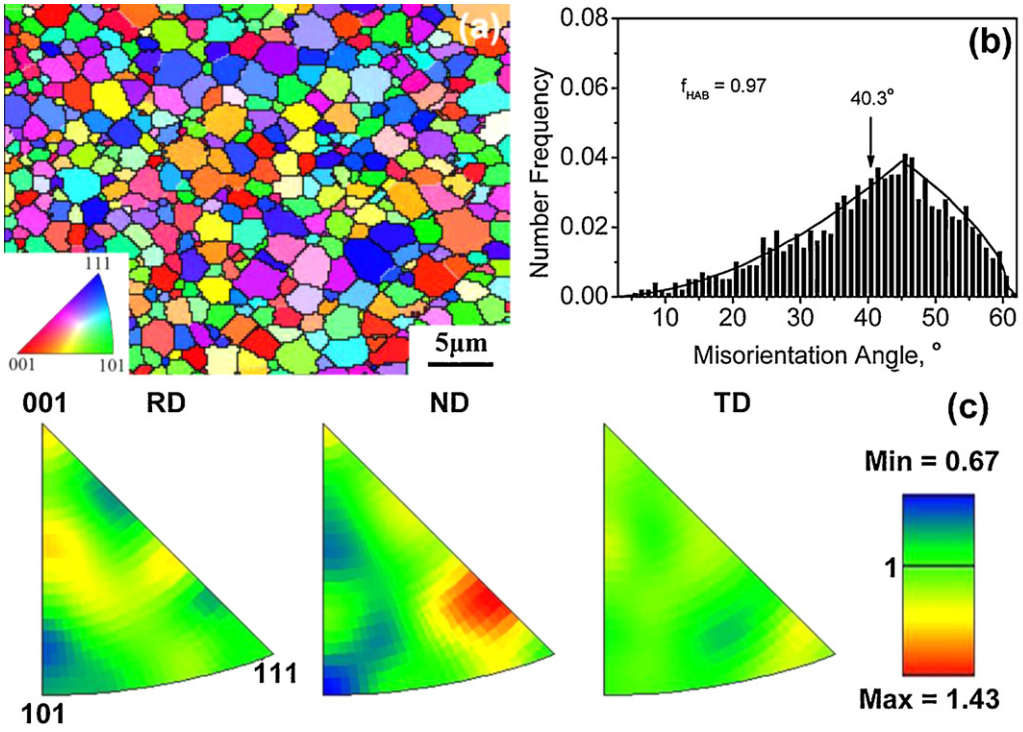

Fig. 7. Microstructure of FSP Al–Mg–Sc: (a) EBSD map, (b) boundary misorientation angle distribution, and (c) inverse pole figures.

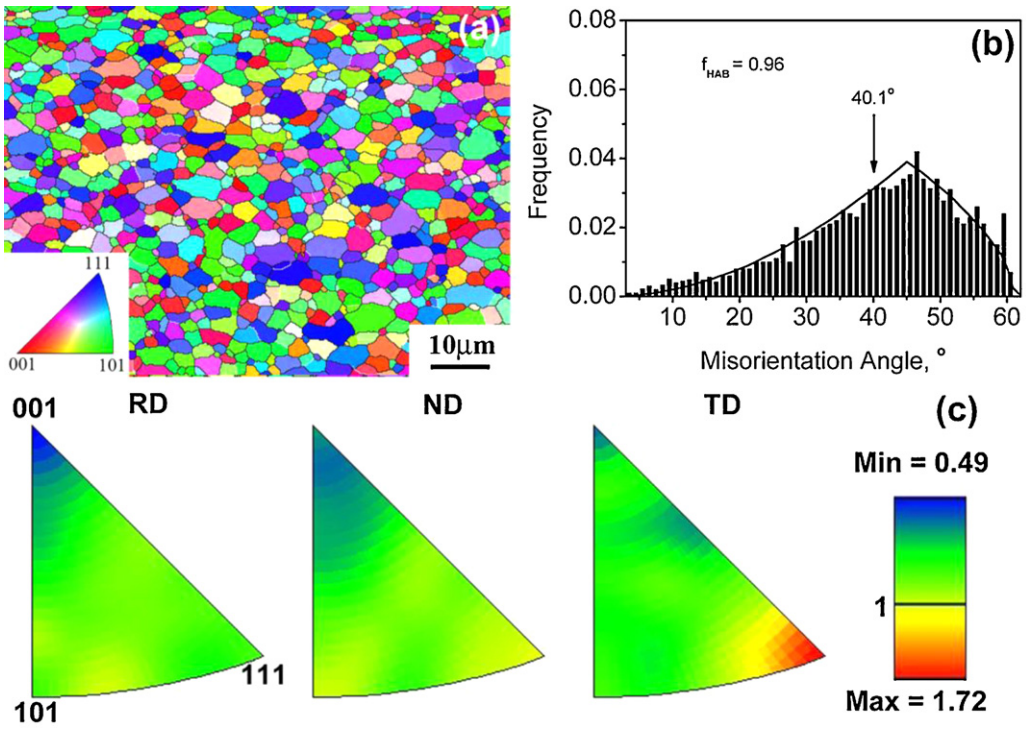

Fig. 8. Microstructure of FSP Al–Mg–Sc deformed to a true strain of 1.4: (a) EBSD map, (b) boundary misorientation angle distribution, and (c) inverse pole figures.

distributions remained almost unchanged and matched well the theoretical distribution [21].

4. Discussion

4.1. Microstructure evolution with flow stress for extruded sample

The microstructural examination showed that the initial banded structure in the as-extruded Al–Mg–Sc was replaced by equiaxed grains with a random misorientation distribution at high strains (Figs. 3–6). A gradual increase in the average misorientation angle and the fraction of HAGBs associated with a randomization of the misorientation distribution occurred during superplastic deformation. These changes are similar to those previously reported for aluminum alloys with initial banded microstructure, such as 8090Al, Al–6Cu–0.4Zr and Sc-modified 7050Al [11,12]. However, the mechanism, as mentioned in the introduction, by which the fine-grained structure is obtained, is still not clear.

Most studies presumed that the initial deformed structure was replaced by new grains with continuous dynamic recrystallization during hot deformation [22–28]. Different models have been developed to predict the microstructure/microtexture evolution based on the transmission electron microscopic observations and EBSD results [22–28]. However, in this study the microstructural evolution of the extruded Al–Mg–Sc was divided into different stages based on the true stress–strain curve and EBSD maps.

4.1.1. Initial strain hardening stage

The as-extruded sample contained a high density of dislocations and subgrain boundaries. During static annealing, the annihilation of dislocations and the rearrangement of dislocations into the surrounding boundaries occurred simultaneously, and at this stage there is little change in the scale of the structure.

During superplastic deformation, the flow stress of the extruded Al–Mg–Sc increased continuously with an increase in the strain in the initial strain range of 0–0.6 (Fig. 2), because the size of the subgrains increased significantly (Figs. 3 and 4). Therefore, this stage was defined as the initial strain hardening stage. As the strain increased from 0 to 0.6, the frequency of boundaries < 5° was reduced and the frequency of boundaries > 50° increased, while the frequency of boundaries in the mid-misorientation range of 15–50° did not show any noticeable change. This trend is consistent with the proposal of threshold misorientation that once the misorientation exceeds 7–8°, the transition into the high misorientation regimes above ~36° occurs rapidly [11].

There are two different mechanisms by which coarsening of the subgrains occurs. One is subgrain boundary migration and the other is subgrain rotation and coalescence [29]. If the subgrain boundary migration occurred alone, the dislocations which formed during the extrusion process were absorbed into the boundaries. This tends to increase the subgrain growth and the misorientation between adjacent grains during superplastic flow [2]. This subgrain growth process is associated with a gradual increase in the boundary misorientation between neighboring grains. In fact, the transition from LAGBs to HAGBs occurred rapidly in this study. The alternative mechanism for subgrain growth is associated with subgrain rotation. Previous in situ TEM observations showed that concurrent straining and annealing substantially accelerated the boundary misorientation increment compared with static annealing [3,30,31]. Deformation to a strain of 0.4 in an extruded Al–Mg–Sc reduced the fraction of LAGBs and introduced boundaries with misorientations higher than 50°, which were rarely observed in the statically annealed samples [30,31]. This misorientation increase trend provides clear evidence for subgrain rotation during the initial stages of superplastic deformation.

The in situ TEM observations by Gudmundsson et al. [3] showed that the dislocation density within the grains of the hot deformed Al–Zr–Si alloy is considerable. This can be interpreted as evidence of an accommodation mechanism for GBS involving the generation

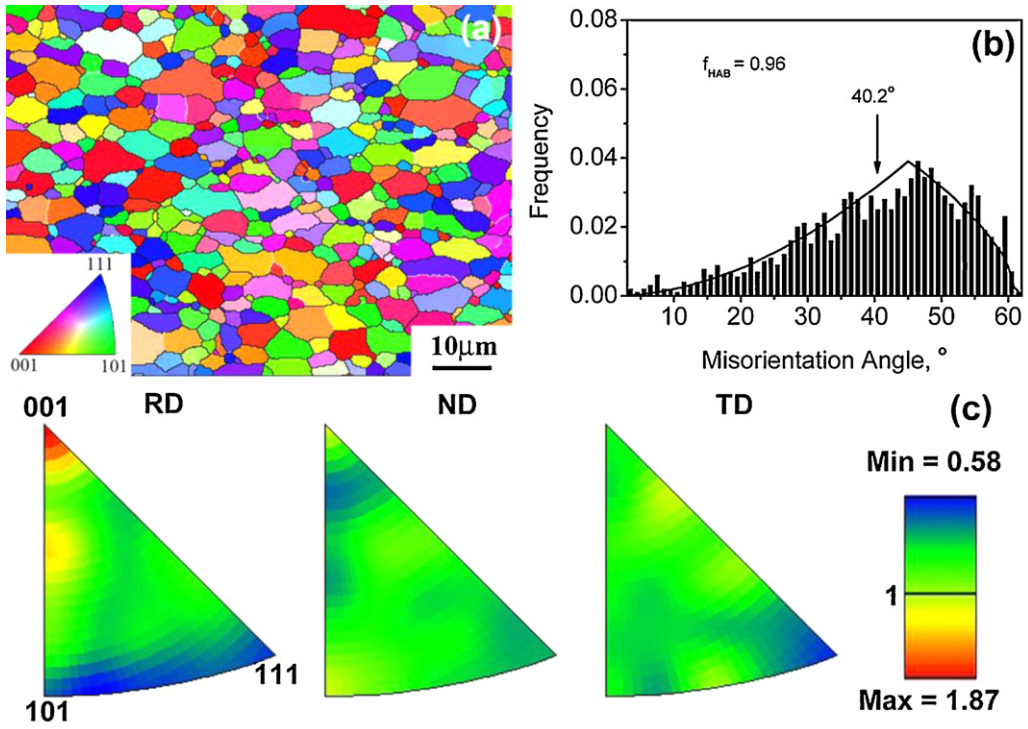

Fig. 9. Microstructure of FSP Al–Mg–Sc deformed to a strain of 3.1: (a) EBSD map, (b) boundary misorientation angle distribution, and (c) inverse pole figures.

and motion of dislocations. They suggested that the grain boundaries with initial misorientations in the range of 5–7° could slide sufficiently to allow an increase in the boundary misorientation. This is contrary to the observations of GBS in bicrystals which showed that GBS hardly occurred for boundary misorientations below 10° [9]. Gudmundsson et al. [3] suggested a more acceptable interpretation of subgrain rotation during concurrent straining and annealing. For alloys containing a fraction of HAGBs before high temperature deformation, sliding along these preexisting HAGBs caused the rotation of the adjoining subgrains, thereby translating LAGBs to HAGBs rapidly throughout the microstructure. Therefore, with an increase in the strain from 0 to 0.6, the subgrain rotation and coalescence appeared to be the dominant deformation mechanism.

4.1.2. Stress maximum

The stress maximum appeared at a strain of 0.6 for the extruded Al–Mg–Sc, indicating a balance between strain hardening and strain softening (Fig. 2). In previous studies, dynamic recrystallization was observed at the stress maximum in many other alloys [32,33]. In this study, the decrease in the maximum texture intensity and the increase of average misorientation with the increase in strain from 0.6 to 1.6 might be a result of dynamic recrystallization, as will be discussed in Section 4.1.3. Dynamic recrystallization led to strain softening, but the subgrain growth resulted in strain hardening. When the effect of strain hardening and strain softening achieved a balance at a strain of 0.6, the stress maximum was observed in the σ–ε curve.

4.1.3. Strain softening stage I

With the increase in strain from 0.6 to 1.6, the flow stress of the extruded Al–Mg–Sc continuously decreased and the strain-hardening exponent continuously decreased from 0 to −0.45 (Fig. 2). The banded microstructure became less well defined at a strain of 1.6 (Fig. 5). The microstructure was characterized by fine recrystallized grains. A previous study has shown that the orientation correlation associated with the initial banded structure would be completely eliminated if the deformation was accomplished by GBS after a tensile strain of 0.5 [34]. The present experimental results showed that retained banding was still readily discernable in many regions. For example, areas of ⟨1 1 1⟩ grains were retained in region I of Fig. 5a. These provided evidence that GBS is not a dominant mechanism during this stage. A similar microstructure change was also observed in 8090Al and Al–Cu–Zr by Bate et al. [12,34]. They asserted that structural development could be better explained solely on the basis of dynamic grain growth and orientation dispersal rather than GBS.

In the present study, the size of the fine grains at a strain of 1.6 is smaller than the size of the subgrains at a strain of 0.6 (Figs. 4 and 5). Therefore, the theories that the fine grains mainly grow from the subgrains could not account for the microstructure evolution as the strain increased from 0.6 to 1.6. During hot deformation, dynamic recrystallization refined the grain size and increased the misorientation, which decreased the flow stress by favoring GBS and grain rotation. Dynamic grain growth increases the flow stress for the coarsening of the grain size. The ideal GBS at a constant strain rate will result in a steady flow stress. In fact, significant strain softening was observed at the strain range of 0.6–1.6 (Fig. 2). This indicates that dynamic recrystallization is very likely to be the main deformation mechanism during this stage, which could account for the decrease in flow stress during this stage.

4.1.4. Strain softening stage II

When the strain was higher than 1.6, the flow stress of the extruded Al–Mg–Sc still decreased as the strain increased, but the strain-hardening exponent is almost constant. Therefore, an inflexion which is indicated by the intersection of the two dashed lines in Fig. 2 appeared in the true stress–strain curve at a strain of 1.6. With the increase of the strain from 1.6 to 2.1 (Figs. 5 and 6), the grains of the deformed specimens tended to become equiaxed in shape, and the distribution of the grains became random. Besides, the average size of the grains increased significantly. These demonstrated that the main deformation mechanism in this stage is GBS and dynamic

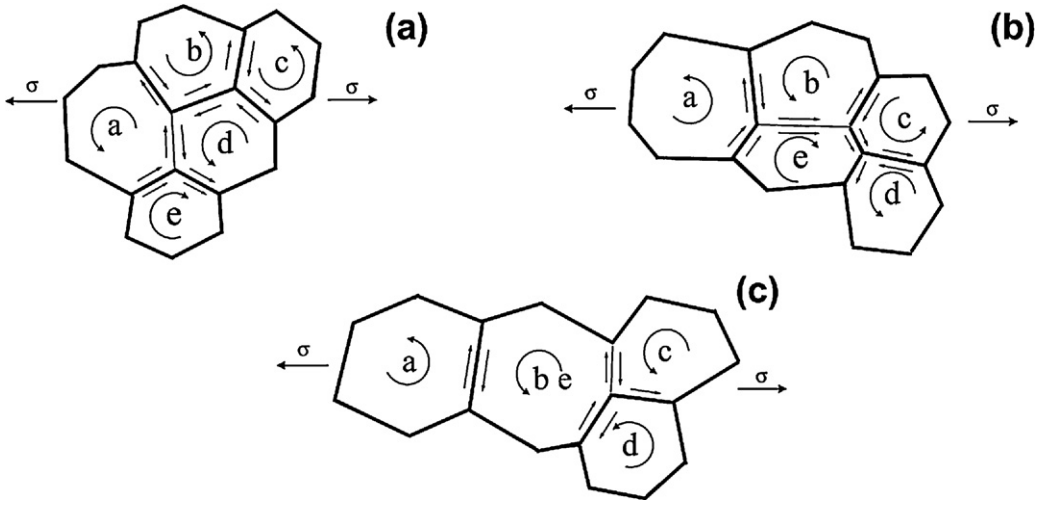

Fig. 10. Schematic representations of microstructural evolution during superplastic deformation accommodated by GBS and dynamic grain growth.

grain growth. The decreasing rate of strain-hardening exponent was reduced at this stage mainly due to the significant dynamic grain growth. However, the σ–ε curve still exhibited a slight lean downwards to the ε axis. This can be attributed to two factors. First, the true strain rate of the tensile specimen decreased as the strain increased because the tensile specimen was pulled at a constant crosshead speed. Second, at higher strains, the non-uniform deformation of the specimen resulted in the assumed cross-section being larger than the real one. Therefore, the calculated true stress in the curve was lower than the real one.

The average misorientation angle and the fraction of HAGBs increased as the strain increased from 1.6 to 2.1 (Figs. 5 and 6). The misorientation distribution tended to be random and the grains approached an equiaxed shape. The maximum texture density was reduced to 1.81. These are the features of a random GBS, and further confirmed the high contribution of GBS during this stage. It should be noted that although the grain boundary characteristics were capable of sliding after the grain boundary migration, the average grain size of the extruded alloy reached ~15 μm, which is much higher than the fine grain size (≤10 μm) required for superplastic deformation. Therefore, the extruded Al–Mg–Sc failed at a strain of 2.1.

4.2. Microstructural evolution with flow stress for FSP sample

The microstructural evolution of the FSP Al–Mg–Sc is relatively simple compared to the extruded sample. By increasing the strain, the grains retained a random distribution, but the average grain size increased significantly and the grains were somewhat elongated along the tensile direction (Figs. 7–9). The misorientation distribution remained almost unchanged and matched well the theoretical distribution [21]. A very weak, almost random texture was observed at different strains. It has been well documented that the main deformation mechanism of FSP aluminum alloys is GBS [20,35]. The microstructural evolution observed in the present study demonstrated that the main deformation mechanism of the FSP Al–Mg–Sc during superplastic deformation is unchanged and always GBS and dynamic grain growth.

As shown in Fig. 2, the FSP Al–Mg–Sc showed a long strain hardening stage up to a rather high strain in the σ–ε curve. Such a curve is typical of FSP alloys undergoing dynamic grain growth during superplastic deformation [15,18,36]. However, for conventional fine-grained superplastic alloys prepared by equal-channel angular pressing or cold rolling, the σ–ε curve usually exhibited a peak stress at a relatively low strain followed by an extensive strain softening stage [5,37]. This difference can be mainly attributed to the fact that the FSP alloys contain a higher fraction of HAGBs and a lower density of dislocations than the conventional fine-grained superplastic alloys. The σ–ε curve of the FSP Al–Mg–Sc exhibited a strain softening at strains higher than 1.4. The explanation for this phenomenon is the same as that for the extruded sample at strains higher than 1.6. The decreased real strain rate and non-uniform deformation of the specimen are responsible for the apparent strain softening phenomenon at higher strains.

4.3. Microstructure evolution during GBS for FSP sample

The microstructural evolution of the FSP Al–Mg–Sc indicated that the grain distribution remained random during superplastic deformation. No preferential orientation was observed during GBS deformation. The number fraction of LAGBs remained constant. This is inconsistent with the microstructural evolution in the extruded sample and the previous studies where the misorientation of the grain boundaries increased with the increase in strain during superplastic deformation [5–11]. A deformation model is needed to explain these occurrences.

When GBS occurred under a driving force at high temperature, this process is accommodated by stress-directed diffusion along the grain boundaries, which resulted in a shape change of the grains [38,39]. Grain rotation (GR) also occurred during deformation due to the shear stresses, caused by GBS and elastic anisotrophy, surrounding the grains [40,41]. Meanwhile, the grain separation and growth which accompanied the shape change were accommodated by GBS and GR to maintain the microstructural coherency [42]. Molecular-dynamic simulation showed that both mechanisms of grain growth, i.e. those involving either curvature-driven grain boundary migration or GR induced grain coalescence, are enhanced by the presence of the applied stress [41].

Based on previous works [16,19,38–41] and the EBSD maps in this study, schematic representations of microstructural evolution during superplastic deformation, accommodated by GBS and dynamic grain growth for the FSP alloys, are proposed, as shown in Fig. 10. The initial fine and equiaxed grains are randomly distributed. The bold lines denote HAGBs, whereas the fine lines denote LAGBs. In the framework of our model, the combined action of the GBS and dynamic grain growth is realized as follows. Because most of the boundary misorientations are high values, GBS proceeds easily along these HAGBs accompanied by the random grain rotations during superplastic deformation. Most of LAGBs are transformed to HAGBs due to the GBS and random grain rotations, while

parts of HAGBs are simultaneously changed to LAGBs, as indicated in Fig. 10a and b. Besides, dynamic grain growth and grain shape change also occur to accommodate the superplastic deformation to avoid the formation of cavities (Fig. 10c).

The present model indicates that the texture is further weakened and the boundary misorientations tend to be randomly distributed during superplastic deformation. For materials with a high fraction of LAGBs, the transformation ratio from LAGBs to HAGBs is much higher than that from HAGBs to LAGBs. In this case, these materials exhibited a monotonic translation from LAGBs to HAGBs from the view of statistics. On the other hand, the microstructure with a random grain misorientation reached a dynamic balance because the transformation ratios from LAGBs to HAGBs and from HAGBs to LAGBs are equivalent.

5. Conclusions

1. A gradual increase in the average misorientation angle and the fraction of HAGBs associated with a randomization of the misorientation distribution occurred in the as-extruded Al–Mg–Sc during superplastic deformation. The initial banded structure in the as-extruded Al–Mg–Sc was replaced by equiaxed grains with a random misorientation distribution at high strains.
2. The microstructural evolution of the extruded Al–Mg–Sc could be divided into three stages. Subgrain rotation and coalescence in the early stage resulted in strain hardening. Dynamic recrystallization in the middle stage accounted for the decrease of flow stress. The main deformation mechanism in the final stage was GBS and dynamic grain growth.
3. The grains in the FSP Al–Mg–Sc remained randomly distributed at various strains, but increased significantly in size with an increase in strain. The dominant deformation mechanism of the FSP Al–Mg–Sc was always GBS and dynamic grain growth during superplastic deformation.
4. A deformation model is developed to illustrate the microstructural evolution during superplastic deformation accommodated by GBS and dynamic grain growth in the FSP alloys. The microstructure with the random grain misorientations reaches a dynamic balance because the transformation ratios from LAGBs to HAGBs and from HAGBs to LAGBs are equivalent during superplastic deformation.

Acknowledgments

The authors gratefully acknowledge (a) the support of the National Natural Science Foundation of China under grant nos. 50871111, 50671103 and 50890171, (b) the National Outstanding Young Scientist Foundation of China under grant no. 50525103.

References

[1] J.W. Edington, K.N. Melton, C.P. Cutler, Prog. Mater. Sci. 21 (1976) 63–170.
[2] S.J. Hales, T.R. Mcnelley, Acta Metall. 36 (1988) 1229–1239.
[3] H. Gudmundsson, D. Broooks, J.A. Wert, Acta Metall. Mater. 39 (1991) 19–35.
[4] T. Mohri, M. Mabuchi, M. Nakamura, T. Asahina, H. Iwasaki, T. Aizawa, K. Higashi, Mater. Sci. Eng. A 290 (2000) 139–144.
[5] R. Kaibyshev, E. Avtokratova, A. Apollonov, R. Davies, Scr. Mater. 54 (2006) 2119–2124.
[6] E. Nes, J. Mater. Sci. Lett. 13 (1978) 2052–2055.
[7] E. Nes, Mater. Sci. 13 (1979) 211–215.
[8] R.H. Bricknell, J.W. Edington, Acta Metall. Mater. 27 (1979) 1303–1311.
[9] P. Lagarde, M. Biscondi, Can. Metall. Q. 13 (1974) 245–251.
[10] H. Gudmundsson, D. Brooks, J.A. Wert, Acta Metall. Mater. 39 (1991) 19.
[11] J. Liu, D.J. Chakrabarti, Acta Mater. 44 (1996) 4647.
[12] P.S. Bate, F.J. Humphreys, N. Ridley, B. Zhang, Acta Mater. 53 (2005) 3059–3069.
[13] W.M. Thomas, E.D. Nicholas, J.C. Needham, M.G. Murch, P. Templesmith, C.J. Dawes, GB Patent Application No. 9125978.8, December 1991.
[14] R.S. Mishra, Z.Y. Ma, Mater. Sci. Eng. Rep. 50 (2005) 1–78.
[15] R.S. Mishra, M.W. Mahoney, S.X. McFadden, N.A. Mara, A.K. Mukherjee, Scr. Mater. 42 (2000) 163–168.
[16] Z.Y. Ma, R.S. Mishra, M.W. Mahoney, Acta Mater. 50 (2002) 4419–4430.
[17] F.C. Liu, Z.Y. Ma, L.Q. Chen, Scr. Mater. 60 (2009) 968–971.
[18] I. Charit, R.S. Mishra, Acta Mater. 53 (2005) 4211–4223.
[19] F.C. Liu, Z.Y. Ma, Scr. Mater. 62 (2010) 125–128.
[20] Z.Y. Ma, R.S. Mishra, M.W. Mahoney, Acta Mater. 50 (2002) 4419–4430.
[21] J.K. Mackenzie, Biometrika 45 (1958) 229–240.
[22] S. Gourdet, F. Montheillet, Acta Mater. 51 (2003) 2685–2699.
[23] X. Zhang, M.J. Tan, Scr. Mater. 38 (1998) 827–831.
[24] K. Tsuzaki, X.X. Huang, T. Maki, Acta Mater. 44 (1996) 4491–4499.
[25] Q. Liu, X.X. Huang, M. Yao, J.F. Yang, Acta Metall. Mater. 40 (1992) 1753–1762.
[26] M. Eddahbi, T.R. Mcnelley, O.A. Ruano, Metall. Mater. Trans. A 32 (2001) 1093–1102.
[27] T.R. Mcnelley, D.L. Swisher, M.T. Perez-Prado, Metall. Mater. Trans. A 33 (2002) 279–290.
[28] M.T. Lyttle, J.A. Wert, J. Mater. Sci. 29 (1994) 3342–3350.
[29] F.J. Humphreys, M. Hatherly, Recrystallization and Related Annealing Phenomena, Elsevier Ltd. Press, 2004, pp. 188–210.
[30] T.R. McNelley, E.W. Lee, M.E. Mills, Metall. Trans. 17A (1986) 1035–1041.
[31] E.W. Lee, T.R. McNelley, A.F. Stengel, Metall. Trans. 17A (1986) 1043–1050.
[32] H.J. Mcqueen, E. Evangelista, J. Bowles, G. Crawford, Metal. Sci. 18 (1984) 395–402.
[33] K.J. Gardner, R. Grimes, Metal. Sci. 13 (1977) 216–222.
[34] P.S. Bate, N. Ridley, B. Zhang, Acta Mater. 55 (2007) 4995–5006.
[35] Z.Y. Ma, F.C. Liu, R.S. Mishra, Acta Mater. 58 (2010) 4693–4704.
[36] F.C. Liu, B.L. Xiao, K. Wang, Z.Y. Ma, Mater. Sci. Eng. A 527 (2010) 4191–4196.
[37] M. Furukawa, A. Utsunomiya, K. Matsubara, Z. Horita, T.G. Langdon, Acta Mater. 49 (2001) 3829–3838.
[38] R.L. Coble, J. Appl. Phys. 34 (1963) 1679–1682.
[39] H.W. Green, J. Appl. Phys. 41 (1970) 3899–3902.
[40] V. Paidar, S. Takeuchi, Acta Metall. Mater. 40 (1992) 1773–1782.
[41] A.J. Haslam, D. Moldovan, V. Yamakov, D. Wolf, S.R. Philpot, H. Gleiter, Acta Mater. 51 (2003) 2097–2112.
[42] B.N. Kim, K. Hiraga, K. Morita, Acta Mater. 53 (2005) 1791–1798.